

Temperature Dependence of Adsorption and Effectiveness for a Pyrimidinium-Type Corrosion Inhibitor on Mild Steel

Yi He,* Shuai Ren,* Xi Wang,* David Young,* Maalek Mohamed-Said,** Bernardo Augusto Farah Santos,* Maria Eduarda Dias Serenario,* and Marc Singer^{†,*}

In the oil and gas industry, produced water with a high dissolved salt content is a common byproduct of hydrocarbon extraction from conventional and unconventional wells. Other than salts, corrosive gases such as CO₂ are abundant in the production stream, which dissolve and acidify the solution, posing a risk of internal pipeline corrosion. To mitigate this issue, injection of corrosion inhibitors has emerged as a cost-effective approach. In various aggressive conditions, heterocyclic molecules that contain nitrogen atoms have proven to be highly effective corrosion inhibitors for many alloys. In this study, tetrahydropyrimidinium (THP-C14) inhibition efficiencies were investigated at temperatures of 25°C, 55°C, and 80°C using electrochemical methods, including linear polarization resistance and potentiodynamic sweeps. Corrosion inhibition data were then correlated with THP-C14 concentration, using the five adsorption isotherms: Langmuir, Temkin, Frumkin, Flory-Huggins, and Dhar-Flory-Huggins models. These isotherms utilize different assumptions to establish the correlation between coverage and inhibitor concentration. The suitability of these five isotherm models for describing the corrosion inhibition behavior of THP-C14 was examined. In addition, the thermodynamic parameters (K_{ad} , $\Delta_{ad}G^{\circ}$) of adsorption for THP-C14 at 25°C, 55°C, and 80°C were calculated and compared using the aforementioned adsorption isotherm models. Finally, a mechanism was proposed for the adsorption behavior of the THP-C14 corrosion inhibitor model compound. Chloride ions were important for inhibitor adsorption.

KEY WORDS: adsorption isotherms, CO₂corrosion, corrosion inhibitor, elevated temperature, inhibition efficiency, mild steel

INTRODUCTION

In the oil and gas industry, produced water is commonly encountered in the process of extracting hydrocarbons from oil and gas wells, which may contain high contents of dissolved salts. Other than salts, corrosive gases such as CO₂ exist in the production stream, which dissolve in the produced water, acidify the solution, and have the potential to result in an internal corrosion of pipelines.¹ To mitigate this issue, the injection of corrosion inhibitors has emerged as a widely adopted and cost-effective approach. Corrosion inhibitor molecules in the brine form protective films on the water-wetted metal surfaces, where corrosion could take place. These films effectively retard electrochemical reaction rates at the interface between water and metal.² Commercial corrosion inhibitors typically contain amphiphilic active ingredients.³ The polar head groups of these molecules promote their interactions with metal surfaces and their hydrophobic tails prevent corrosive species from approaching the surface. In various aggressive conditions, heterocyclic molecules that contain nitrogen atoms have proven to be highly effective corrosion inhibitors for many alloys.⁴⁻⁶

Exploring the influence of elevated temperatures on inhibition performance poses challenges related to experimental methods and environment control.⁷ In a study conducted by Ding⁷ adsorption kinetics were characterized using

imidazoline-type and quaternary ammonium-type corrosion inhibitors within the temperature range of 25°C to 80°C. The results of the study indicated that the decrease in inhibition efficiency (IE) at higher temperatures was due to desorption being favored at those conditions.

In general, inhibitor adsorption occurs via physisorption (involving electrostatic attraction between the charged metal surface and the charged inhibitor molecules) and/or via chemisorption (involving charge sharing or charge transfer from inhibitor molecules to the surface leading to the formation of a coordinate-type bond, akin to a Lewis interaction).⁸⁻⁹ The former could be assisted by the presence of chloride ions in oil and gas extraction fields.¹⁰ The chloride ions could act as a linkage between the positively charged surface and cationic inhibitor heads to support the physisorption so that the inhibitor can keep working efficiently.¹⁰ The latter may occur if the inhibitor contains lone pairs of electrons, multiple bonds, or a conjugated π -type bond system.¹¹⁻¹³

Bentiss, et al.,¹⁴ investigated how the corrosion behavior of mild steel was affected in the presence of a thiazole-type corrosion inhibitor from 30°C to 60°C under acidic conditions. Their findings demonstrated that the IE increased with temperature and linked this to the onset of chemisorption, which suggested that chemisorption was preferred to physisorption at elevated temperatures. However, the study did not provide further explanation about how the temperature-dependent

Submitted for publication: April 11, 2023. Revised and accepted: December 18, 2023. Preprint available online: December 20, 2023, <https://doi.org/10.5006/4346>.

[†] Corresponding author. E-mail: singer@ohio.edu.

* Institute for Corrosion and Multiphase Technology, Department of Chemical and Biomolecular Engineering, Ohio University, Athens, Ohio, 45701.

** TotalEnergies, OneTech, CSTJF, Avenue Larribau, F-64018 Pau, France.

Table 1. Elemental Composition (wt%) of Carbon Steel C1018

Element	Cr	Mo	S	V	Si	C	Ni	Mn	P	Fe
wt%	0.076	0.015	0.026	0.001	0.21	0.15	0.027	0.63	0.011	Balance

behavior was linked to the nature of chemisorption. Zhang, et al.,¹⁵⁻¹⁶ evaluated the IE of three imidazoline derivatives with halogen substitutions at various temperatures (30°C to 70°C) in an HCl solution for mild steel. Two of the corrosion inhibitors had decreased effectiveness while the third one had essentially unchanged performance at higher temperatures. These three corrosion inhibitors mainly exhibited physisorption on the metal surfaces, however, the effect of temperature on corrosion inhibition was not straightforward and varied depending on the corrosion inhibitor. Whether chemisorption or physisorption is dominant is not only determined by the corrosion inhibitor chemistry and substrate material but also by the temperature and chemistry of the environment. In addition, the knowledge regarding the impact of temperature on adsorption and the effectiveness of pyrimidinium-type corrosion inhibitors is insufficient. It is important to note that our study focuses solely on adsorption and does not take into account any possible thermal degradation effects of chemicals.

Many corrosion inhibitor studies utilize the criteria based on the standard adsorption Gibbs energy $\Delta_{ad}G^\circ$ to distinguish between physisorption and chemisorption.¹⁷⁻¹⁹ When $\Delta_{ad}G^\circ$ exceeds -20 kJ/mol, the interaction between surfactant and metal is commonly categorized as physisorption.¹⁷⁻²⁰ When $\Delta_{ad}G^\circ$ is between -80 kJ/mol and -400 kJ/mol, the interaction between surfactant and metal is associated with chemisorption.²¹⁻²² The adsorption isotherms can give important information on the interaction of inhibitor and metal surface. The values of $\Delta_{ad}G^\circ$ are not absolute and fixed thresholds applicable to all systems. Instead, they are general trends that have been observed in various adsorption processes, and they serve as rough guidelines to differentiate between physisorption and chemisorption based on the strength of interactions. Solmaz, et al.,²³ tested different adsorption isotherms to find the most suitable adsorption isotherm for the adsorption of 2-mercaptothiazoline on the mild steel surface from 0.5 M HCl solution. They found that the Langmuir adsorption isotherm was more suitable than other isotherm models at room temperature. They also calculated $\Delta_{ad}G^\circ$ based on the K_{ad} (equilibrium constant of adsorption/desorption). According to the $\Delta_{ad}G^\circ$ value, a conclusion has been made that the inhibitor was physisorbed on the metal surface by the formation of an adsorptive film with an electrostatic character. Kumar²⁴ conducted a comprehensive study comparing the accuracy of linear and nonlinear fitting methods in estimating sorption isotherm parameters for malachite green adsorption onto activated carbon at four different solution temperatures of 32°C, 40°C, 50°C, and 60°C. By comparing nonlinear sum of square error parameter estimates vs. linearizing the form of the isotherm, he demonstrated the superiority of the nonlinear fitting method, highlighting its efficacy in obtaining reliable isotherm parameters. The problem with linearization is that it does not uniformly weigh the experimental data. Yet, the assumptions associated with a specific isotherm model should be carefully assessed to make sure

they correspond to the adsorption behavior of inhibitor molecules on the steel surface in the studied conditions.²⁵

The corrosion inhibitor model compound used in this work is known as tetradecyl-1,4,5,6-tetrahydropyrimidinium (THP-C14), which contains a pyrimidine structural moiety.²⁶ This compound is commonly found in specific commercial corrosion inhibitor formulations used in refinery systems. Experiments were conducted under various conditions, including different corrosion inhibitor concentrations and temperatures, to investigate both the corrosion inhibition and adsorption behavior. This study focuses on a high salt concentration condition that simulates the exploration and production environments in the oil and gas industry.²⁷ A parallel study has recently been published concerning condensed water in gas production, which has low salt content and lack of CO₂.²⁸ In this study, the IE were investigated at temperatures of 25°C, 55°C, and 80°C using electrochemical methods, including linear polarization resistances (LPR) and potentiodynamic polarization sweeps. Corrosion inhibition data was related to surface coverage with THP-C14 concentration. The corrosion inhibition behavior was analyzed using the five adsorption isotherms, namely, the Langmuir, Temkin, Frumkin, and Flory-Huggins/Dhar-Flory-Huggins models, which correlated coverage and corrosion inhibitor concentration based on different assumptions.^{9,29} The suitability of these isotherms was assessed by considering both their goodness of fit and the appropriateness of the underlying assumptions. Furthermore, the thermodynamic parameters (K_{ad} , $\Delta_{ad}G^\circ$) of the adsorption for the THP-C14 at 25°C, 55°C, and 80°C were calculated and compared by using different adsorption isotherm models. Finally, a mechanism was proposed for the adsorption behavior of the THP-C14 corrosion inhibitor model compound. This paper is the full-length version of a recently published conference proceeding.³⁰

EXPERIMENTAL PROCEDURES

2.1 | Materials and Chemicals

The electrochemical measurements were conducted on specimens of carbon steel (C1018, UNS G10180⁽¹⁾). These specimens exhibited a microstructure characterized by a combination of ferrite and pearlite. The composition of this carbon steel was shown in Table 1. The electrolyte solution consisted of 5 wt% (0.86 M) sodium chloride (NaCl), which was then saturated with carbon dioxide (CO₂) under a total pressure of 1 bar and temperatures of 25°C, 55°C, and 80°C to simulate CO₂ corrosion conditions; this also facilitated deoxygenation. 0.86 M sodium perchlorate (NaClO₄) was also used in some experiments to simulate similar ionic strength in 0.86 M NaCl solution.

In this study, the corrosion inhibitor model compound utilized was THP-C14. The synthesis of THP-C14 was performed as a bromide salt, following the procedures outlined in an earlier publication.²⁶ The chemical structure of THP-C14, as depicted in Figure 1, features a delocalized positive charge straddling two nitrogen atoms separated by carbon in the head group. The product THP-C14 exhibited a purity of approximately 99% determined by ¹H-NMR, as described in the prior paper.²⁶

⁽¹⁾ UNS numbers are listed in *Metals & Alloys in the Unified Numbering System*, published by the Society of Automotive Engineers (SAE International) and cosponsored by ASTM International.

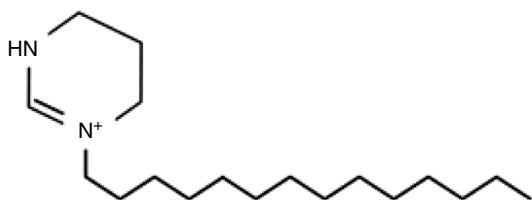


FIGURE 1. Molecular structure of 1-tetradecyl-1,4,5,6-tetrahydropyrimidinium (THP-C14).

2.2 | Electrochemical Measurements

The electrochemical experiments were conducted using a three-electrode setup.²⁶ A rotating cylinder electrode (RCE) made of C1018 carbon steel was used as the working electrode (exposed area 2.89 cm²) in the experiments. The counter electrode was a platinum mesh and the reference electrode was Ag/AgCl saturated with KCl. Before each experiment, the RCE was polished with silicon carbide abrasive papers of 240, 400, and 600 grit in isopropanol flow, followed by cleaning in an ultrasonic isopropanol bath and drying in lab air. The solution was sparged with CO₂ for 2 h in a sealed 2 L glass cell before the introduction of the RCE.²⁶ The RCE was then inserted into the glass cell and rotated at 1,000 rpm controlled by a modulated speed rotator.⁽²⁾ Solution pH was adjusted to 4.50±0.05 using deoxygenated hydrochloric acid or sodium bicarbonate solution before each experiment and maintained at this value during the entire exposure time. The C1018 specimen was conditioned with 20 min of precorrosion, and an initial corrosion rate (CR) was collected and compared with a blank test (0 ppm of corrosion inhibitor) to ensure no inhibitor contamination from the previous experiment. The inhibitor was added after 20 min of precorrosion. For CR assessment, the LPR was measured using a potentiostat⁽³⁾ with a scan range of -5 mV_{OCP} to +5 mV_{OCP} (open-circuit potential [OCP]), using a scan rate of 0.125 mV/s, and the solution resistance were compensated for. Solution resistance was determined at the high-frequency range of the electrochemical impedance spectrum collected at the beginning of the experiment. Then, the polarization resistance from the LPR method was compensated for the solution resistance using the aforementioned value. The B value used in both inhibited and uninhibited experiments was 26 mV, derived from prior research that investigated the behavior of mild steel in a CO₂ environment.¹⁰ The B value for inhibited and uninhibited conditions could be different due to the change of dominance of mass transfer and charge transfer on cathodic reaction. However, for the sake of simplicity of CR calculation, the B value of 26 mV was consistently applied to analyze all of the experimental data reported in this study. Potentiodynamic polarization curves were also collected at the end of the experiments. The cathodic polarization was collected from OCP to -0.7 V_{OCP}, while the anodic polarization was from OCP to +0.3 V_{OCP}. Various concentrations of corrosion inhibitors were tested, and each experiment was repeated at least twice.

RESULTS AND DISCUSSION

3.1 | Effect of Temperature on Surface Saturation Concentration

A series of inhibition experiments were conducted using various concentrations of THP-C14 to establish the relationship between inhibitor concentrations and CR at different

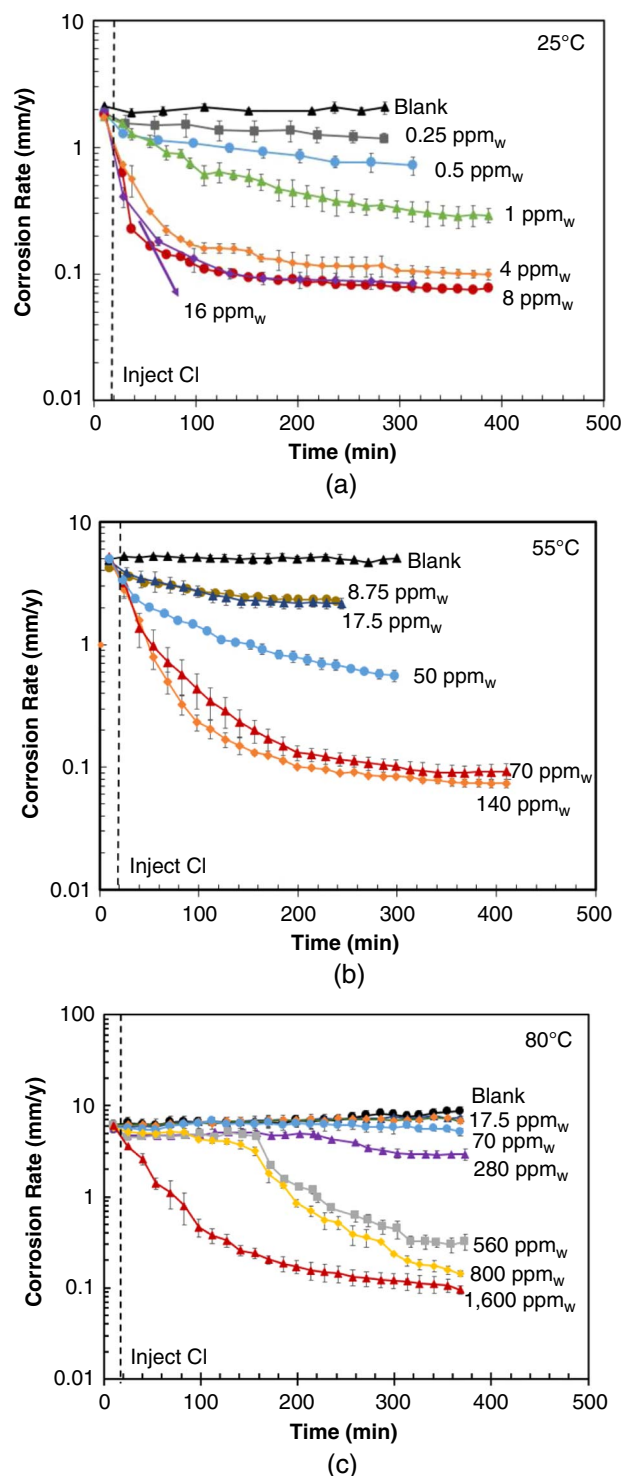


FIGURE 2. The CR of the C1018 carbon steel in the presence and absence of THP-C14 at (a) 25°C (b) 55°C, and (c) 80°C as a function of time. The error bars represent the max and min values of repeated experiments.

temperatures. As shown in Figure 2(a), at 25°C, the CR was 2.01±0.13 mm/y with no corrosion inhibitor. As the concentration of THP-C14 increased from 0.25 ppm_w to 4 ppm_w, the CR exhibited a reduction, ultimately reaching approximately 0.1 mm/y. Upon exceeding a concentration of 4 ppm_w, the CR remained consistently at 0.11±0.02 mm/y and did not

⁽²⁾ Pine Research, Durham, NC.

⁽³⁾ Reference 600+, Gamry Instruments, Warminster, PA.

change significantly with the further increase in corrosion inhibitor concentration. According to Murakawa, et al.,³¹ corrosion inhibitors keep adsorbing onto the metal surface until the corrosion inhibitor reaches a saturation point, where introducing more corrosion inhibitors to the bulk solution does not lead to a further reduction in CR. The concentration of the corrosion inhibitor required to achieve this saturation point is termed the surface saturation concentration (SSC).³¹ Therefore, the SSC of the THP-C14 model compound was found to be between 1 ppm_w and 4 ppm_w.²⁶ Based on the analysis of the data presented in Figures 2(b) and (c), it was determined that the SSC of THP-C14 at 55°C and 80°C ranged from 50 ppm_w to 70 ppm_w and 800 ppm_w to 1,600 ppm_w, respectively. These results indicated that the SSC of THP-C14 significantly increased with temperature.

The range of corrosion inhibitor dosage needed at 80°C was high for an actual pipeline mitigation strategy, however, the objective of the current study was not to develop a highly effective corrosion inhibitor but to understand the inhibition mechanism at elevated temperatures. Therefore, investigations were performed even if the corrosion inhibitor dosage was high. In Figure 2(c), at a temperature of 80°C, the CR exhibited an incubation period that corresponded to the onset of corrosion inhibitor effectiveness for concentrations in the range of 17.5 ppm_w to 800 ppm_w. However, unlike the lower dosage, there was no observable incubation time with 1,600 ppm_w THP-C14. This was similar to what was observed at lower temperatures, 25°C and 55°C in Figures 2(a) and (b), where no incubation time was observed even at low inhibitor concentration. As temperature increases, based on the Arrhenius rate law, the adsorption and desorption constants increase, leading to an increase in the rate of both adsorption and desorption processes.³²⁻³⁴ Therefore, the equilibrium constant of adsorption and desorption is temperature-dependent as well. In this study, the desorption rate increased at a greater rate than the adsorption rate, even though the adsorption process remained dominant. Therefore, more time may be needed to establish a protective inhibitor layer on the metal surface. An increase in the concentration of the corrosion inhibitor leads to higher availability of inhibitor molecules, thereby reducing the time required for the onset of inhibition.

Figure 3 illustrates the potentiodynamic polarization sweeps for CO₂ corrosion of C1018 carbon steel at temperatures of 25°C, 55°C, and 80°C, with different THP-C14 concentrations. At 25°C, as shown in Figure 3(a), when the concentration of corrosion inhibitor was increased from 0 ppm_w to 4 ppm_w, the corrosion current reduced, which suggested the improved inhibition effect upon inhibitor adsorption.³⁵ Both anodic and cathodic reactions were retarded upon higher inhibitor concentrations, but OCPs shifted to more positive potentials, which indicated that anodic reactions were retarded to a greater extent compared to cathodic reactions. However, the limiting currents remained unaffected, likely because the adsorbed inhibitor layer was too thin to affect the diffusion of hydrogen ions. In addition, the difference between the polarization curves of 4 ppm_w and 8 ppm_w was negligible, because further reduction of cathodic and anodic reactions above SSC would be trivial. At 55°C as shown in Figure 3(b), when the concentration of corrosion inhibitor was decreased from 70 ppm_w to 0 ppm_w, the polarization curves shifted rightward with cathodic limiting current unaffected, which was similar to what was observed at 25°C. At 80°C in Figure 3(c), compared with the blank test, the presence of corrosion inhibitor also retarded both the anodic and

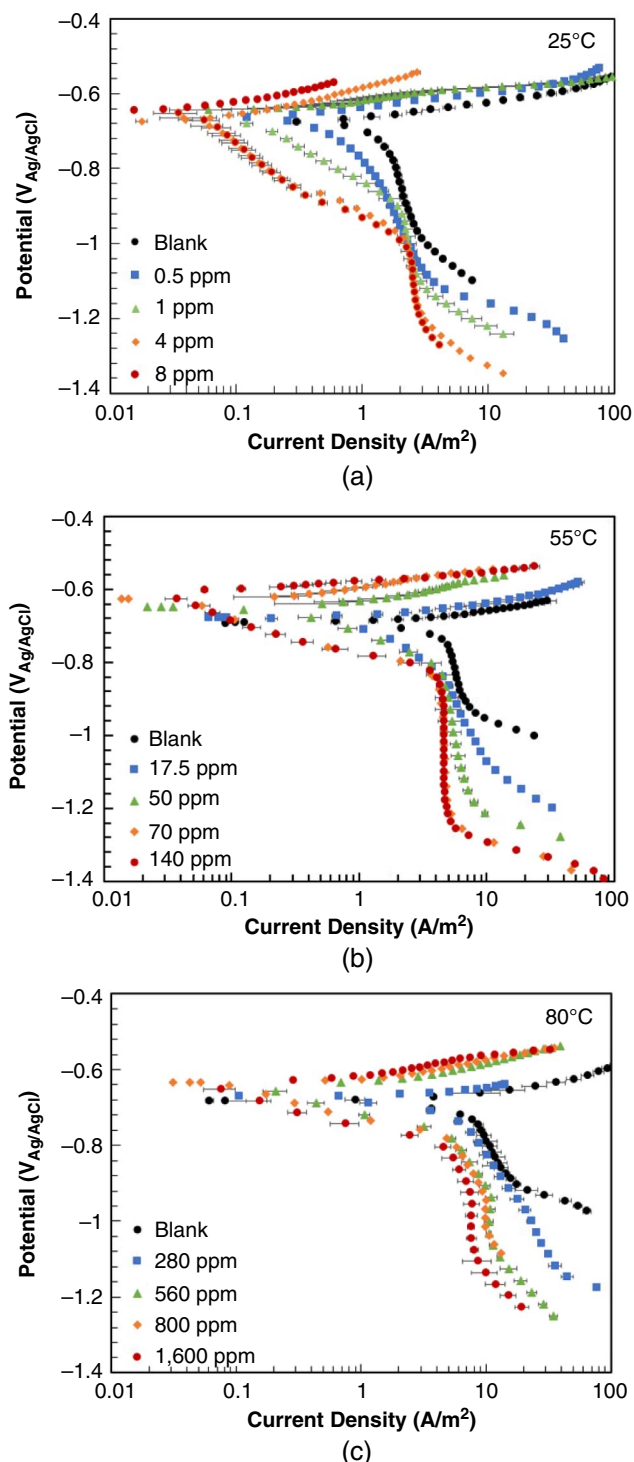


FIGURE 3. Potentiodynamic polarization curves of C1018 in 5 wt% NaCl solution at (a) 25°C, (b) 55°C, and (c) 80°C with different THP-C14 concentrations. The error bars represent the max and min values of repeated experiments.

reactions. However, the limiting current shifted in the 1,600 ppm_w condition (Figure 3(c)), which was a noticeable deviation from what was observed at lower temperatures (Figures 3(a) and (b)). With 1,600 ppm_w inhibitor, the formed inhibitor layer could be thick enough to decrease the mass transfer of corrosive species to the metal surface.

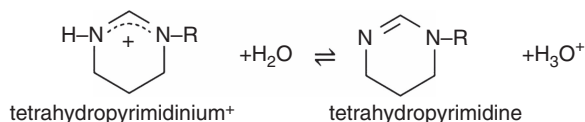
3.2 | Effect of Temperature on Inhibition Efficiency

The CR was continuously monitored until it reached a stable state, characterized by a minimal variation of less than ± 0.01 mm/y between consecutive measurements. The corrosion inhibition efficiency (IE) was determined utilizing Equation (1)³⁶

$$IE = 1 - \frac{CR_0}{CR} \quad (1)$$

where CR_0 represents the CR in the presence of the corrosion inhibitor and CR is the corrosion rate in the absence of the corrosion inhibitor. To evaluate the impact of temperature on the inhibition performances of THP-C14, a comparison of inhibition behaviors was conducted at 25°C, 55°C, and 80°C. As shown in Figure 4, IE decreased as the temperature increased at a fixed concentration of corrosion inhibitor. To achieve optimal inhibition performance, higher corrosion inhibitor concentrations were necessary at 80°C. Moreover, as shown in both Figures 2(c) and 4, the inhibitor lost its IE at 80°C with 17.5 ppm_w and 70 ppm_w.

One possible reason for the inhibitor losing IE at elevated temperatures could be the inhibitor's deprotonation behavior. Protonation/deprotonation behavior, chemically expressed by an acid dissociation constant, i.e., K_a value, is important³⁷ for describing the characteristics of THP-C14. As mentioned previously,²⁶ the protonated THP-C14 head group (tetrahydropyrimidinium) can dissociate into tetrahydropyrimidine and hydrogen ions, as expressed in the following reaction with formed hydronium ($R: -C_{14}H_{29}$).



The equilibrium expression for this dissociation reaction is shown in Equation (2)

$$K_a = \frac{[\text{tetrahydropyrimidine}][\text{H}_3\text{O}^+]}{[\text{tetrahydropyrimidinium}^+]} \quad (2)$$

From this, the derived Henderson-Hasselbalch equation for tetrahydropyrimidinium⁺ can be written as Equation (3). This is useful for determining relative concentrations of species associated with THP-C14 at given pH values; partial dissociation, resulting in a balance between the undissociated acid and its conjugate base.

$$\text{pH} = \text{p}K_a + \log \frac{[\text{tetrahydropyrimidine}]}{[\text{tetrahydropyrimidinium}^+]} \quad (3)$$

The calculated $\text{p}K_a$ value associated with the THP-C14 head group is 12.5⁽⁴⁾ at room temperature. The magnitude of this $\text{p}K_a$ value implies that the tetrahydropyrimidinium (THP-C14) is a weak acid that will overwhelmingly remain in its protonated form at pH values well below 12.5. At pH 4.5, the THP-C14 corrosion inhibitor model compound is protonated; it possesses a cationic head group, which adsorbs on the metal surface. Due to the endothermicity of weak acid dissociation,³⁸ the concentration of tetrahydropyrimidinium in solution will decrease with the increase of temperature. Therefore, it can be argued that more

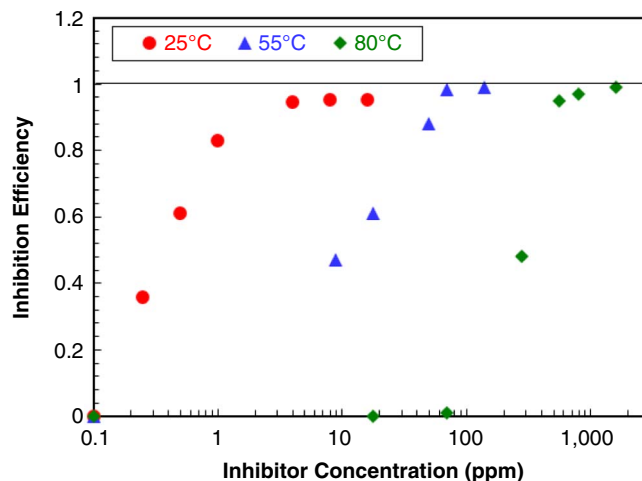


FIGURE 4. Changes of IE with different THP-C14 concentrations at 25°C, 55°C, and 80°C.

THP-C14 dosage was likely needed to obtain better inhibition performance at high temperatures. Although $\text{p}K_a$ value of THP-C14 is only available at 25°C, it may not change significantly with temperature.³⁸⁻³⁹ Therefore, such an effect is likely to be minor when compared against the governing kinetic parameters.

One can speculate that as temperature increases, whether the more intense corrosion activities could be inhibited or not depends on the adsorption kinetics of the inhibitor. If the inhibitors exhibit physisorption on the metal surface, the desorption kinetics could be faster than adsorption with increasing temperature, so the inhibition could be lost at high temperatures. If the inhibitors exhibit chemisorption on the metal surface, the bonding between inhibitors and the metal surface is strong and will not easily break upon increasing temperature, so the inhibition could be retained even at elevated temperatures.

3.3 | Fitting of Different Adsorption Isotherms at 25°C, 55°C, and 80°C

Adsorption isotherms provide information about adsorption and desorption equilibrium, which helps understand the inhibition change upon temperature. Hence, the inhibition experimental results were used to fit adsorption isotherms. Considering the wide range of available adsorption isotherms, it is important to carefully choose the most appropriate model that can best describe the adsorption and desorption process of THP-C14 molecules on the surface of carbon steel, taking into account the specific conditions being studied.⁴⁰⁻⁴¹ This evaluation section aimed to assess five adsorption isotherm models by fitting them to the experimental data obtained under steady-state conditions with various inhibitor concentrations (C_{inh}). The experimental data involved various inhibitor concentrations (C_{inh}) plotted against the equilibrium fractional coverage (θ_{eq}), as shown in Figure 5. To calculate θ_{eq} , Equation (4) proposed by Murakawa, et al.,³¹ was utilized

$$\theta_{eq} = \frac{(i_{corr})_{\theta=0} - (i_{corr})_{\theta}}{(i_{corr})_{\theta=0} - (i_{corr})_{\theta=\max}} \quad (4)$$

where $(i_{corr})_{\theta=0}$ represents the steady-state CR in the absence of corrosion inhibitor, $(i_{corr})_{\theta}$ is the steady-state CR in the presence of corrosion inhibitor, and $(i_{corr})_{\theta=\max}$ refers to

⁽⁴⁾ Advanced Chemistry Development (ACD/Labs) Software V11.02 (© 1994-2022 ACD/Labs).

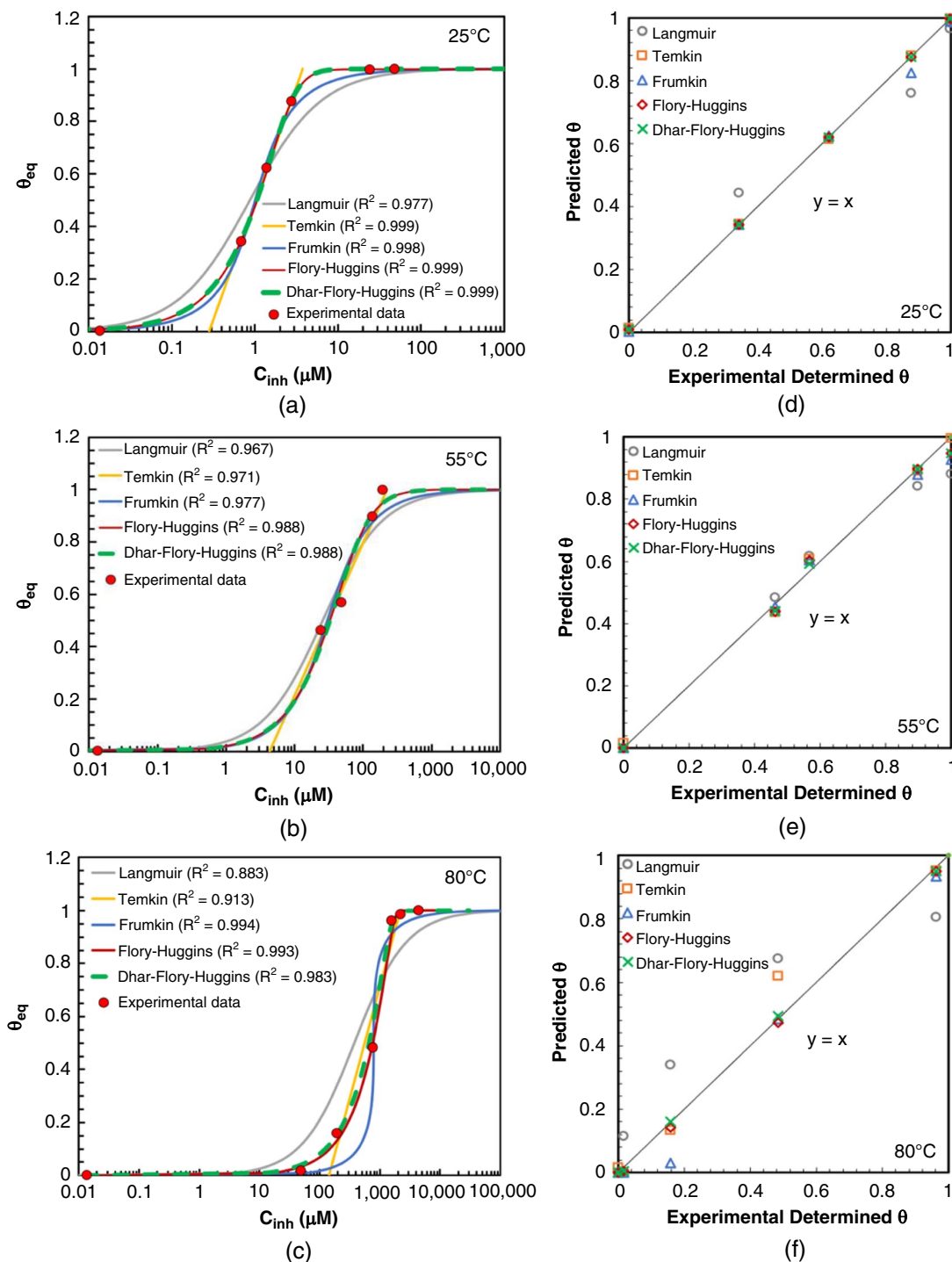


FIGURE 5. Comparison of adsorption isotherm models with experimental data with various THP-C14 concentrations and temperatures at (a) 25°C, (b) 55°C, and (c) 80°C. (d) through (f) are experimentally determined surface coverages and predicted surface coverages based on different adsorption isotherms.

the steady-state CR when inhibitor concentration reaches the SSC, with the maximum coverage on the metal surface.

Some literature^{9,42-43} used a linear regression method on an isotherm model, but that could introduce errors carried along with the fitting process.⁴⁴ Therefore, our experimental data were fitted with the nonlinear equations of each isotherm model to determine the constants in the equations. Nonlinear regression functions were utilized to minimize the sum of the

squares of the differences between experimental data and the calculated one obtained from various isotherm models. As a result, the fitting routine yielded the optimized constant values, as well as the goodness of fitting (R^2 coefficient). In Figure 5, the fitting curves obtained by the various adsorption isotherm models are displayed for temperatures of 25°C, 55°C, and 80°C. The inhibitor concentrations that could provide 50% coverage increased with the increasing

temperature, which matched the increasing trend of SSC in Figure 2. By fitting the steady-state experimental data, the equilibrium constant of adsorption/desorption (K_{ad}), the fitting factor (R^2), and other model-specific constants in the isotherm model were determined at these temperatures (Table 2).

3.3.1 | Langmuir Isotherm Model

This model assumes a homogeneous surface with a monolayer of adsorbed inhibitor molecules, without any interactions among them. The equation below illustrates the relationship between concentration and surface coverage^{9,45-46}

$$C_{inh}K_{ad} = \left(\frac{\theta_{eq}}{1 - \theta_{eq}} \right) \quad (5)$$

where C_{inh} is the bulk concentration of corrosion inhibitor. K_{ad} is the equilibrium constant for the adsorption/desorption process. θ_{eq} represents the steady-state coverage of the surface at specific concentrations of corrosion inhibitor.

Table 2 shows that the Langmuir model provided a good fit for the experimental data at both 25°C and 55°C, as indicated by the high values of the fitting factor (R^2) and Figures 5(d) and (e), but a not so good fit at 80°C. In addition, the predicted coverage typically overestimates with lower inhibitor concentrations and underestimates with higher inhibitor concentrations, especially at 80°C.

3.3.2 | Temkin Isotherm Model

This model assumes that the surface is heterogeneous, consisting of numerous small areas, each of which follows the Langmuir isotherm without any molecular interactions.⁴⁷ The relationship between concentration and surface coverage is shown in the following equation⁴⁸

$$K_{ad}C_{inh} = e^{g\theta} \quad (6)$$

where g is the adsorbent-adsorbate interaction constant. For a reliable and linear adsorption isotherm plot, surface coverages should fall within the linear window for inhibitor adsorption, i.e., 0.2 to 0.8.⁴⁸ However, limited experimental data fell in this range, so the selection was then extended to $0.1 < \theta < 0.9$. Nevertheless, based on results from Figures 5(d) through (f) and Table 2, the Temkin model provided a good fit for the experimental data at 25°C, 55°C, and 80°C, with fitting factor (R^2) higher than 0.9, and predicted coverages agreed well with experimental results.

3.3.3 | Frumkin Isotherm Model

This model is based on the assumption that the surface is heterogeneous and that lateral interactions between the adsorbed surfactant molecules need to be taken into account.⁴⁷ The Frumkin isotherm is described by Equation (7)

$$K_{ad}C_{inh} = \frac{\theta_{eq}}{1 - \theta_{eq}} \exp(-f\theta_{eq}) \quad (7)$$

where the constant f represents the interactions between the adsorbate molecules and remains unaffected by surface coverage θ . The Langmuir model is a particular example of the Frumkin model, in which the constant f is set to zero.

The Frumkin isotherm fit the experimental data well at 25°C, 55°C, and 80°C, except low concentration range at 80°C, as shown in Figure 5. The positive f value at 25°C, 55°C, and 80°C in Table 2 indicates the existence of repulsive interactions between adsorbed species.⁴⁹ The different f values are attributed to differences in the orientation of the adsorbed species.⁴⁹

Table 2. Evaluation of Equilibrium Constant (K_{ad}), Coefficient of Determination (R^2), and Other Parameters Through Fitting Experimental Data with Different Adsorption Models at Different THP-C14 Concentrations at 25°C, 55°C, and 80°C

Temperature (°C)	Adsorption Model	Equilibrium Constant and Fitting		Other Parameters
		K_{ad} (L/ μ mol)	R^2	
25	Langmuir	1.14	0.977	–
	Temkin	3.55	0.999	$g = 2.60$
	Frumkin	0.379	0.998	$f = 1.93$
	Flory-Huggins	2.06	0.999	$\delta = 0.279$
	Dhar-Flory-Huggins	1.18	0.999	$\delta = 0.279$
55	Langmuir	3.86×10^{-2}	0.967	–
	Temkin	23.1×10^{-2}	0.971	$g = 3.94$
	Frumkin	1.85×10^{-2}	0.977	$f = 1.16$
	Flory-Huggins	4.29×10^{-2}	0.988	$\delta = 0.503$
	Dhar-Flory-Huggins	3.54×10^{-2}	0.988	$\delta = 0.503$
80	Langmuir	2.66×10^{-3}	0.883	–
	Temkin	7.03×10^{-3}	0.913	$g = 2.74$
	Frumkin	1.74×10^{-4}	0.994	$f = 3.99$
	Flory-Huggins	9.88×10^{-3}	0.993	$\delta = 0.0699$
	Dhar-Flory-Huggins	1.99×10^{-3}	0.983	$\delta = 0.0999$

Note: δ is the number of solvent molecules substituted by one adsorbate molecule, g is the adsorbent-adsorbate interaction constant, and f is the adsorbate interaction constant.

3.3.4 | Flory-Huggins and Dhar-Flory-Huggins Isotherm Model

These models consider the substitution of adsorbed solvents by adsorbing molecules.⁴⁷ Unlike the Flory-Huggins model, the Dhar-Flory-Huggins isotherm includes an exponential factor. As shown in Equations (8) and (9)

$$\text{Flory-Huggins : } K_{\text{ad}}C_{\text{inh}} = \frac{\theta_{\text{eq}}}{\delta(1 - \theta_{\text{eq}})^{\delta}} \quad (8)$$

$$\text{Dhar-Flory-Huggins : } K_{\text{ad}}C_{\text{inh}} = \frac{\theta_{\text{eq}}}{e^{(\delta-1)}(1 - \theta_{\text{eq}})^{\delta}} \quad (9)$$

where δ represents the number of solvent molecules that are displaced by an adsorbate molecule. The Langmuir model is a particular example of both the Flory-Huggins and Dhar-Flory-Huggins models, where δ is equal to 1.

For Flory-Huggins and Dhar-Flory-Huggins isotherms, both fit the experimental data well at 25°C, 55°C, and 80°C, as shown in Figure 5. However, the value of δ , which represents the number of solvent molecules (water for this study) substituted by an adsorbate molecule (corrosion inhibitor for this study), is less than 1, as shown in Table 2. The expected value should be higher than 1 because the size of the corrosion inhibitor is much higher than the water molecule. The same phenomenon is also observed by Baikerikar and Hansen.⁵⁰ The size ratio they obtained was about 0.5, whereas the expected value was 3. The physical basis underlying Flory-Huggins and Dhar-Flory-Huggins isotherm models is weak for interaction parameters as large as encountered in aqueous-organic solute systems. The significance or meaning of fractional numbers of δ , in this case, is difficult to understand from a chemical and/or phenomenological point of view.⁸ There are still challenges in understanding the physical meanings of the constants in the different model equations, a subject of ongoing research.

When the temperature was increased to 80°C, the Langmuir model exhibited poor fitting performance (Figures 5[c] and [f]), whereas the other isotherm models (Temkin, Frumkin, Flory-Huggins, and Dhar-Flory-Huggins) showed better fitting performance. This difference in performance could be attributed to the formation of THP-C14 films and show a multilayer character on the metal surface at elevated temperatures, rendering the Langmuir model inapplicable in this case. It is noteworthy that all of the isotherm models are developed based on specific assumptions. The selection of an isotherm is often based on some statistical analysis (e.g., R^2).^{24,43} However, the goodness of the curve fitting may not offer any insight into possible adsorption mechanisms. How to select an isotherm for an adsorption study remains a big challenge due to the extremely complex adsorption mechanisms. Because the determination of the equilibrium constant of adsorption closely

depends on the isotherm equation used, for a given set of adsorption data, values of the equilibrium constant K_{ad} determined by using different adsorption models would vary significantly.

3.4 | Adsorption Mechanisms at 25°C, 55°C, and 80°C

The adsorption mechanisms of corrosion inhibitors can be classified as physisorption, chemisorption, or a combination thereof.²⁰ The first inhibitor layer adsorbed on the solid surface could be either physically or chemically adsorbed, but the second layer should be present via physisorption.²⁰ In this scenario, the adsorption process is a combination of chemisorption and physisorption. One of the most important assessment criteria to categorize the adsorption mechanism is the determination of $\Delta_{\text{ad}}G^{\circ}$ (standard adsorption Gibbs energy), which was shown in the equation below.^{48,51}

$$\Delta_{\text{ad}}G^{\circ} = -RT\ln(K_{\text{ad}}) \quad (10)$$

where $\Delta_{\text{ad}}G^{\circ}$ is standard free energy change, R is the universal gas constant $8.314 \text{ J}\cdot\text{mol}^{-1}\cdot\text{K}^{-1}$, and T is the absolute temperature. K_{ad} is the equilibrium constant of adsorption/desorption with the unit of $\text{L}/\mu\text{mol}$, which could be converted into a dimensionless constant by multiplying it by $55.5 \text{ mol water per liter}$ (i.e., $1,000 \text{ g}$ divided by the weight of pure water).^{9,21} The values of K_{ad} for 25°C, 55°C, and 80°C were summarized in Table 2. Using Equation (10), adsorption-free energy at different temperatures can be obtained. These thermodynamic estimates can offer insight into the type and mechanism of an adsorption process. Table 3 shows the changes in $\Delta_{\text{ad}}G^{\circ}$ value at different temperatures by using different adsorption isotherm models. As can be seen from Table 3, the inhibitor adsorption process has negative values of $\Delta_{\text{ad}}G^{\circ}$, which indicates spontaneous adsorption of THP-C14 on the metal surface.⁵² From Table 3, when the temperature increased from 25°C to 80°C, $\Delta_{\text{ad}}G^{\circ}$ also increased, regardless of the isotherms used, and shows a trend to become closer to -20 kJ/mol , above which the interaction between surfactant and metal is often classified as physisorption.²¹⁻²² This indicated that when the temperature increased, it was more likely that THP-C14 underwent a physisorption process.²¹⁻²² The values of $\Delta_{\text{ad}}G^{\circ}$ are not absolute and fixed thresholds applicable to all systems. Instead, they are general trends that have been observed in various adsorption processes, and they serve as rough guidelines to differentiate between physisorption and chemisorption based on the strength of interactions.¹⁷⁻¹⁹ However, there are still some challenges to categorizing the adsorption behavior based solely on $\Delta_{\text{ad}}G^{\circ}$, because it does not directly identify the nature of the adsorption-related interaction at the metal surface. Further understanding of inhibitor-metal interaction is necessary. Previous research showed that chloride ions could act as a linkage between the positively charged surface and cationic inhibitor heads, so the inhibitor could adsorb on the metal

Table 3. Changes of $\Delta_{\text{ad}}G^{\circ}$ Value at Different Temperatures by Using Different Adsorption Isotherm Models

Temperature (°C)	Standard Adsorption Gibbs Energy, $\Delta_{\text{ad}}G^{\circ}$ (kJ/mol)				
	Langmuir	Temkin	Frumkin	Flory-Huggins	Dhar-Flory-Huggins
25	-44.6	-47.3	-41.7	-45.9	-44.5
55	-39.7	-42.8	-37.7	-40.1	-39.4
80	-34.9	-37.8	-26.9	-38.7	-34.1

surface via physisorption and keep working efficiently.^{10,53-54} To examine if such linkage occurs between THP-C14 and steel surface, additional experiments controlling chloride concentrations were performed.

Not all anionic species are expected to facilitate the adsorption of inhibitor molecules. Although the presence of halide ions enhancing the performance of inhibitors was observed in some studies, other anions, such as ClO_4^- have no impact on IE.^{53,55} 0.86 M NaClO_4 (0 M NaCl) was used in this work, which corresponds to the same anion concentration in the 0.86 M NaCl solution, creating a similar ionic strength. After the inhibitor was introduced in the NaClO_4 solution, chloride ions would be introduced gradually to reveal its effect on inhibitor adsorption. As shown in Table 4, the result showed that the injection of a 4 ppm corrosion inhibitor in the pure NaClO_4 solution did not significantly change the carbon steel CR. This indicates that the inhibitor did not function in the perchlorate solution effectively as in the chloride solution, which was likely because perchlorate ions, as opposed to chloride ions, did not significantly coordinate on the metal surface.⁵⁶⁻⁵⁷ As shown in Table 4, the test solution was initially only aqueous NaClO_4 , then NaCl was added gradually. When 0.02 M NaCl was then added, a slight decrease in CR was observed. A further increase in NaCl concentration to 0.17 M resulted in a more pronounced decrease in CR. When even more NaCl was added, sufficient to achieve 0.86 M NaCl, a further decrease in CR was observed before its stabilization was achieved at ca. 0.13 mm/y, which was comparable with the inhibited corrosion rate in the pure 0.86 M NaCl solution. The result indicated that the presence of Cl^- was crucial for the adsorption of corrosion inhibitor molecules. In addition, the above experiments were conducted in the absence of divalent cations (e.g., $\text{Ca}^{2+}/\text{Mg}^{2+}$) and the impact of a complex brine needs to be investigated in the future.

Figure 6 illustrates the proposed adsorption mechanism of the THP-C14 corrosion inhibitor model compound. When the metal surface is positively charged with respect to potential of zero charge,¹⁰ surface active anions, such as chloride ions, Cl^- , play a critical role in the adsorption of cationic inhibitors. Ding⁷ demonstrated that the presence of Cl^- ions was necessary for the adsorption of a cationic (imidazolium type) inhibitor on a carbon steel surface. The author proposed that the positively charged surface would repel the cationic inhibitor due to electrostatic repulsion but that the Cl^- ions could act as a ligand between the surface and the inhibitor.¹⁰ With more Cl^- in the solution and adsorbed on the metal surface, more corrosion inhibitors will be adsorbed to the adsorbed Cl^- layer (and consequently to the metal surface) and form a barrier to a corrosive environment, thus further decreasing the CR. It is

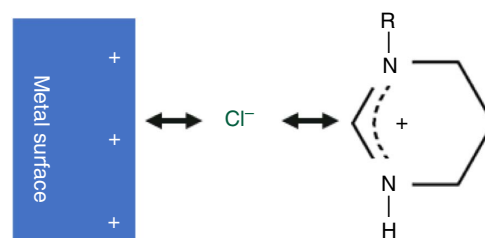


FIGURE 6. Postulated adsorption mechanism for the THP-C14 inhibitor model compound, R represents an aliphatic alkyl tail (R: $-\text{C}_{14}\text{H}_{29}$).

also hypothesized that the bonding between the steel surface, the Cl^- ions, and the cationic inhibitor is physical in nature, via electrostatic attractions between charged molecules and the metallic surface. The adsorption of Cl^- facilitates the subsequent physisorption of cationic inhibitors, by acting as the linkage between the positive charge surface and the positively charged cationic inhibitor molecule. This work speculates the physisorption of THP-C14 on carbon steel surfaces based on electrochemical results. More atomistic level studies, such as time of flight secondary ion mass spectroscopy, and molecular simulations, should be conducted in the future to further understand the inhibitor-metal interaction.

CONCLUSIONS

This inhibition study utilized THP-C14 to inhibit C1018 corrosion in a pH 4.5, CO_2 saturated, and 5 wt% NaCl electrolyte from 25°C to 80°C. As a result of this study, the following conclusions were drawn:

- > The IE decreased as the temperature increased at a fixed concentration of corrosion inhibitor. To achieve optimal inhibition performance, higher corrosion inhibitor concentrations were necessary at 80°C.
- > All investigated isotherms, including Langmuir, Temkin, Frumkin, Flory-Huggins, and Dhar-Flory-Huggins, provided a good fit for surface coverage at temperatures of 25°C and 55°C. When the temperature was increased to 80°C, the Langmuir model exhibited poor fitting performance, whereas the other isotherm models showed better fitting performance. The underlying reason for this behavior change is still being investigated, but it may be attributed to differences in the corrosion inhibitor film structure.
- > The thermodynamic parameters (K_{ad} , $\Delta_{\text{ad}}G^\circ$) of the adsorption for the studied inhibitor are calculated and compared by using different adsorption isotherm models at different temperatures. When the temperature increased from 25°C to 80°C, $\Delta_{\text{ad}}G^\circ$ also increased, and THP-C14 underwent a physisorption process.
- > The THP-C14 inhibitor model compound has a high pK_a value, which makes it mostly protonated in acidic to neutral environments.
- > The THP-C14 inhibitor model compound is physisorbed to the surface steel via electrostatic attractions between the charged inhibitor molecules and the charged metallic surface. Chloride ions play a critical role in inhibitor adsorption. With more Cl^- in the solution, more corrosion inhibitor molecules will adsorb on the metal surface and form a protective layer, thus further decreasing the corrosion rate.

ACKNOWLEDGMENTS

This project has been supported by TotalEnergies transversal R&D project (MANA WELLS R&D Programs). The authors would

Table 4. The Inhibited and Uninhibited Corrosion Rates of C1018 at 25°C in pH 4.5 CO_2 Environment with 0.86 M NaClO_4

Solution Composition			Final Steady-State CR (mm/y)
NaClO_4 (M)	NaCl (M)	THP-C14 (ppm)	
0.86	0	0	1.17±0.18
0.86	0	4	1.01±0.13
0.86	0.02	4	0.43±0.07
0.86	0.17	4	0.24±0.03
0.86	0.86	4	0.13±0.02

like to thank Alexis Barxias and Cody Shafer for their technical support at the Institute for Corrosion and Multiphase Technology (ICMT) at Ohio University.

References

- M.B. Kermani, D. Harrop, *SPE Prod. Facil.* 11 (1996): p. 186-190.
- Y. Xiong, B. Brown, B. Kinsella, S. Nešić, A. Pailleret, *Corrosion* 70 (2014): p. 247-260.
- Y. Duda, R. Govea-Rueda, M. Galicia, H.I. Beltraén, L.S. Zamudio-Rivera, *J. Phys. Chem. B* 109 (2005): p. 22674-22684.
- V. Otieno-Alego, N. Huynh, T. Notoya, S.E. Bottle, D.P. Schweinsberg, *Corros. Sci.* 41 (1999): p. 685-697.
- D. Chebabe, Z. Ait Chikh, N. Hajjaji, A. Srhiri, F. Zucchi, *Corros. Sci.* 45 (2003): p. 309-320.
- F. Bentiss, M. Lagrenee, M. Traisnel, J.C. Hornez, *Corros. Sci.* 41 (1999): p. 789-803.
- Y. Ding, "Mechanistic Understanding of CO₂ Corrosion Inhibition at Elevated Temperatures" (Ph.D. diss., Ohio University, 2019).
- A.A. El-Awady, B.A. Abd-El-Nabey, S.G. Aziz, *J. Electrochem. Soc.* 139 (1992): p. 2149-2154.
- Y. Zhu, M.L. Free, R. Woollam, W. Durnie, *Prog. Mater. Sci.* 90 (2017): p. 159-223.
- Z. Belarbi, F. Farel, M. Singer, S. Nešić, *Corrosion* 72 (2016): p. 1300-1310.
- E.E. Ebenso, U.J. Ekpe, B.I. Ita, O.E. Offiong, U.J. Ibok, *Mater. Chem. Phys.* 60 (1999): p. 79-90.
- N. Hackerman, *Corrosion* 18 (1962): p. 332t-337t.
- N.E. Idakar, K. Nobe, *Corrosion* 37 (1981): p. 271-278.
- F. Bentiss, M. Lebrini, M. Lagrenée, *Corros. Sci.* 47 (2005): p. 2915-2931.
- K. Zhang, B. Xu, W. Yang, X. Yin, Y. Liu, Y. Chen, *Corros. Sci.* 90 (2015): p. 284-295.
- K. Zhang, W. Yang, B. Xu, Y. Liu, X. Yin, Y. Chen, *J. Taiwan Inst. Chem. Eng.* 57 (2015): p. 167-174.
- M. Scendo, *Corros. Sci.* 47 (2005): p. 2778-2791.
- I.B. Obot, N.O. Obi-Egbedi, A.O. Eseola, *Ind. Eng. Chem. Res.* 50 (2011): p. 2098-2110.
- A. Kokalj, *Corros. Sci.* 196 (2022): p. 109939.
- G. Barnes, I. Gentle, *Interfacial Science: An Introduction*, 2nd ed. (New York, NY: Oxford University Press, 2011), p. 163-164.
- P.C. Okafor, Y. Zheng, *Corros. Sci.* 51 (2009): p. 850-859.
- M. Behpour, S.M. Ghoreishi, N. Soltani, M. Salavati-Niasari, M. Hamadani, A. Gandomi, *Corros. Sci.* 50 (2008): p. 2172-2181.
- R. Solmaz, G. Kardaş, M. Çulha, B. Yazici, M. Erbil, *Electrochim. Acta* 53 (2008): p. 5941-5952.
- K.V. Kumar, *J. Hazard. Mater.* 136 (2006): p. 197-202.
- I. Ekemini, A. Onyewuchi, J. Abosedo, *Chem. Sci. Int. J.* 18 (2017): p. 1-34.
- Y. He, S. Ren, X. Wang, D. Young, M. Singer, Z. Belarbi, M. Mohamed-Said, S. Camperos, R. Khan Md, K. Cimatu, *Corrosion* 78 (2022): p. 625-633.
- R.P.W.M. Jacobs, R.O.H. Grant, J. Kwant, J.M. Marquenie, E. Mentzer, "The Composition of Produced Water from Shell Operated Oil and Gas Production in the North Sea," in *Produced Water* (New York, NY: Springer, 1992), p. 13-21.
- Y. He, X. Wang, D. Young, M. Mohamed-Said, S. Ren, M. Singer, *J. Electrochem. Soc.* 170 (2023): p. 111502.
- C. Li, "Effect of Corrosion Inhibitor on Water Wetting and Carbon Dioxide Corrosion in Oil-Water Two-Phase Flow" (Ph.D. diss., Ohio University, 2009).
- Y. He, S. Ren, X. Wang, D. Young, M. Singer, M. Mohamed-Said, S. Camperos, "The Effect of Temperature on the Adsorption Behavior and Inhibition Performance of a Pyrimidine-Type Inhibitor at Medium Temperature Range (25°C to 80°C)," CORROSION 2022, paper no. 17895 (Houston, TX: AMPP, 2022).
- T. Murakawa, S. Nagaura, N. Hackerman, *Corros. Sci.* 7 (1967): p. 79-89.
- R. Gorte, L.D. Schmidt, *Surf. Sci.* 76 (1978): p. 559-573.
- L.T. Novak, D.C. Adriano, *J. Environ. Qual.* 4 (1975): p. 261-266.
- W.H. Kuan, S.L. Lo, C.M. Chang, M.K. Wang, *Chemosphere* 41 (2000): p. 1741-1747.
- Z. Belarbi, J.M. Dominguez Olivo, F. Farel, M. Singer, D. Young, S. Nešić, *Corrosion* 75 (2019): p. 1246-1254.
- S. Papavinasam, "Evaluation and Selection of Corrosion Inhibitors," in *Uhlig's Corrosion Handbook*, 3rd ed. (Hoboken, NJ: John Wiley and Sons, 2011), p. 1121-1127.
- V.K. Rajan, K. Muraleedharan, *IJCR Int. J. Cheminf. Res.* 2 (2016): p. 1-8.
- S. Bergström, G. Olofsson, *J. Solution Chem.* 4 (1975): p. 535-554.
- L. Samuelsen, R. Holm, A. Lathuile, C. Schönbeck, *Int. J. Pharm.* 560 (2019): p. 357-364.
- S. Kalam, S.A. Abu-Khamsin, M.S. Kamal, S. Patil, *ACS Omega* 6 (2021): p. 32342-32348.
- M.A. Al-Ghouti, D.A. Da'ana, *J. Hazard. Mater.* 393 (2020): p. 122383.
- M.M. Osman, E. Khamis, A. Michael, *Corros. Prev. Control* 41 (1994): p. 60-65.
- Z. Latif, A. Fazal, M.A. Choudhary, Z. Ahmad, M.A. Mirza, *Appl. Chem. Eng.* 2 (2019): p. 1-8.
- C.H. Bolster, G.M. Hornberger, *Soil Sci. Soc. Am. J.* 71 (2007): p. 1796-1806.
- I. Langmuir, *J. Am. Chem. Soc.* 40 (1918): p. 1361-1403.
- S. Azizian, S. Eris, L.D. Wilson, *Chem. Phys.* 513 (2018): p. 99-104.
- J. Bockris, A. Reddy, M. Gamboa-Aldeco, *Modern Electrochemistry* (New York, NY: Springer, 2002), p. 938.
- W. Durnie, R. De Marco, A. Jefferson, B. Kinsella, *J. Electrochem. Soc.* 146 (1999): p. 1751-1756.
- C.A. Başar, *J. Hazard. Mater.* 135 (2006): p. 232-241.
- K.G. Baikerikar, R.S. Hansen, *Surf. Sci.* 50 (1975): p. 527-540.
- Y. Liu, *J. Chem. Eng. Data* 54 (2009): p. 1981-1985.
- P.C. Okafor, Y. Zheng, *Corros. Sci.* 51 (2009): p. 850-859.
- K. Aramaki, M. Hagiwara, H. Nishihara, *Corros. Sci.* 27 (1987): p. 487-497.
- E.E. Ebenso, *Mater. Chem. Phys.* 79 (2003): p. 58-70.
- N. Hackerman, E.S. Snavey, J.S. Payne, *J. Electrochem. Soc.* 113 (1966): p. 677.
- T. Murakawa, N. Hackerman, *Corros. Sci.* 4 (1964): p. 387-396.
- S. Gonzalez, M.M. Laz, R.M. Souto, R.C. Salvarezza, A.J. Arvia, *Corrosion* 49 (1993): p. 450-546.